ESKİŞEHİR TEKNİK ÜNİVERSİTESİ BİLİM VE TEKNOLOJİ DERGİSİ B- TEORİK BİLİMLER

Eskişehir Technical University Journal of Science and Technology B- Theoretical Sciences

2019, 7(1), pp. 46 - 58, DOI:10.20290/aubtdb.465445

CHARACTERIZATION OF PbS FILM PRODUCED BY CHEMICAL BATH DEPOSITION AT ROOM TEMPERATURE

Metin KUL

Department of Physics, Science Faculty, Eskişehir Technical University, Eskişehir, Turkey

ABSTRACT

PbS film has been produced by chemical bath deposition (CBD) method onto glass substrates using aqueous solution containing $Pb(NO_3)_2$, Na_2SO_3, NaOH and $SC(NH_2)_2$. The deposition was carried out at room temperature of 26°C and a stirring speed of 60 rpm for an hour. The PbS film has been characterized by x-ray diffraction, field emission scanning electron microscopy, Fourier transform infrared spectroscopy, Raman spectroscopy and optical absorption spectroscopy techniques. The PbS film is polycrystalline face centered cubic phase having randomly preferential orientation in the [101], [200], [220] and [400] directions. The texture coefficient, lattice parameter, strain, crystallite size, and dislocation density were estimated from x-ray diffraction results. Fourier transform infrared result reveals that the presence of PbS and various functional groups in PbS sample. Raman spectrum of the sample shows PbS phase and lead oxysulfates. The optical band gap of the PbS film has been studied using the optical absorbance measurement as a function of wavelength between 200 and 2750 nm. The optical direct band gap of the sample is calculated to be 1.28 eV. The optical band gap of PbS sample exhibited a blue-shift compared with that of bulk PbS.

Keywords: Lead sulfide, XRD, FESEM, Vibrational spectroscopy, Optical band gap

1. INTRODUCTION

Lead sulfide (PbS) films, as one of the important binary IV–VI semiconductors, have attracted considerable attention in the field of optoelectronics applications like thermoelectric devices [1], infrared radiation detectors [2], chemical sensors [3], photographic equipment [4], heterojunction photovoltaic cells [5], light-emitting diodes [6], solar control coatings [7], telecommunications [8]. PbS shows a direct optical band gap with 0.4 eV at room temperature and has a large excitation Bohr radius of 18 nm, which permits quantum confinement effect. The optical band gap of PbS film in nanocrystalline form can be widened to the visible region. PbS crystallizes in the rock salt type structure [9-11]. The pressure can induce a phase transition of PbS from cubic to orthorhombic [12]. Different shapes such as nanocrystals, nanocubes, nanoparticles, nanorods, nanospheres, nanotubes, nanowires, quantum dots for PbS film have been obtained [13]. PbS films generally exhibit a p-type conductivity. Physical and chemical properties of PbS can be changed by Zn, Sb, Mn, Mg, Sr, Ni, Co and Fe dopants [14-16].

PbS samples have been deposited by different methods such as electrodeposition [10], spray pyrolysis [17], SILAR [18], rf sputtering [11], chemical vapour deposition [19] and chemical bath deposition (CBD) [9, 20, 21]. CBD is a technique in which semiconductor films are deposited onto substrates immersed in dilute solutions. The CBD technique has been a more attractive technology which is simple, well suited for large area coating, low temperature processing and low process cost. The major deposition variables are the precursor properties and concentrations, bath temperature and substrates [22].

This work has been concerned with the production and characterization of PbS film using CBD method at room temperature. The structural, morphological and optical properties of PbS film were characterized using x-ray diffraction (XRD), field emission scanning electron microscopy (FESEM), Fourier transform infrared (FTIR) spectroscopy, Raman spectroscopy and optical absorption spectrocopy techniques.

Corresponding Author: mkul@eskisehir.edu.tr
Received: 28.09.2018 Accepted: 03.12.2018

2. EXPERIMENTAL

PbS film was deposited onto microscope glass substrates (76 × 13 × 1mm^3) by the CBD method. The glass substrate was immersed in boiling water with detergent, and then soaked in chromic acid, cleaned in isopropyl alcohol, rinsed in distilled water at each step and finally dried in air. The deposition bath contained 10 ml of 0.01 M $Pb(NO_3)_2$, 10 ml of 2.5x10^{-4} M Na_2SO_3, 10 ml of 0.15 M NaOH, 10 ml of 0.05 M $SC(NH_2)_2$ and 10 ml distilled water to complete the volume to 50 ml. Sodium sulfide which is the least expensive and most active was used to be oxygen scavenger [23, 24]. The glass substrate was placed vertically inside the glass beaker. The solution was stirred at a spin speed of 60 rpm. The deposition was carried out at room temperature of 26°C for 60 min. After the growth procedure, the deposited PbS film to remove some unwanted and loose particles was rinsed lightly in distilled water and then dried in air. The PbS film was deposited onto both sides of the glass substrate. Sulfuric acid was used to remove the film on back side of the substrate. The front side was used for all measurements. The PbS film was uniform, well adherent and dark gray in colour.

The reaction of PbS formation on the glass substrates is given by [25]:

$$\begin{gathered} Pb(NO_3)_2 + 2NaOH \rightarrow Pb(OH)_2 + 2NaNO_3 \\ Pb(OH)_2 + 4NaOH \rightarrow Na_4Pb(OH)_6 \\ Na_4Pb(OH)_6 \rightarrow 4Na^+ + HPbO_2^- + 3OH^- + H_2O \\ SC(NH_2)_2 + OH^- \rightarrow CH_2N_2 + H_2O + SH^- \\ HPbO_2^- + SH^- \rightarrow PbS + 2OH^- \end{gathered} \tag{1}$$

The weight difference method was used to calculate PbS film thickness. In this method, it was assumed that the film on the substrate is homogeneous and dense having 7.6 g/cm^3 density. PbS film thickness was calculated to be 875 nm by this method. Electrical conductivity type of the sample was determined by hot probe method. PbS film exhibits p-type conductivity. The structural characterization of the sample was performed by a Bruker D8 Advance x-ray diffractometer (XRD) system using Cu Kα radiation (1.5406 Å) with a scanning rate of 2° min^{-1}. The operating voltage and the current used for the XRD study are 40 kV and 30 mA, respectively. Surface morphological study was carried out by means of field emission scanning electron microscopy (Carl Zeiss Ultra Plus FESEM). Fourier transform infrared spectrum (FT-IR) was recorded in the region 4000–400 cm^{-1} with Bruker IFS 66 v/S Vacuum FT-IR spectrometer using the KBr pellet technique to determine the chemical structure of the sample. Raman spectrum was recorded with a Bruker Senterra dispersive Raman microscope. A 3B diode laser (532 nm, 10mW) was used as an excitation source. The optical absorption spectrum was recorded using a Solid Spec-3700 DUV spectrophotometer.

3. RESULTS AND DISCUSSION

The XRD pattern of PbS film deposited onto microscope glass substrates has been studied in 2θ ranges from 15° to 75° and is shown in Figure 1. The appearance of sharp peaks reveals that the sample is polycrystalline. The existence of multiple diffraction peaks of (1 1 1), (2 0 0), (2 2 0), (3 1 1), (2 2 2), (4 0 0) (3 3 1), and (4 2 0) indicates the polycrystalline nature of the PbS film with face centered cubic structure on the basis of PDF data (Card No: 01-077-0244). No peak of any other phase such as PbS_2O_3 and $PbSO_3$ is detected in XRD spectrum, implying that the film is pure.

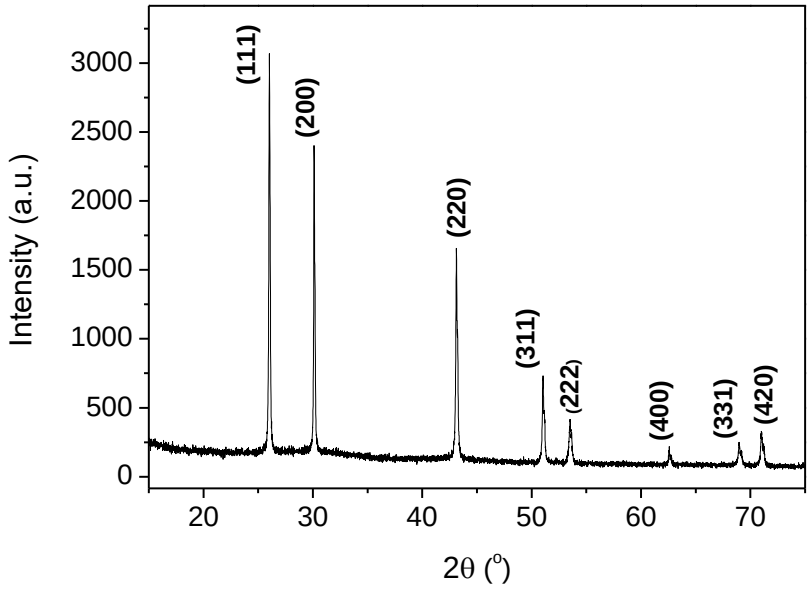


Figure 1. X-ray diffraction pattern of PbS sample

The preferential orientation of the dominant phase of the sample has been determined by means of the texture coefficient (*TC*) using the expression [26],

$$TC(hkl) = \frac{I(hkl)/I_0(hkl)}{(1/N)\sum_N I(hkl)/I_0(hkl)} \quad (2)$$

where *h, k, l* are the miller indices, I_0 (*hkl*) is the standard intensity of the (*hkl*) plane, *I* (*hkl*) is the observed intensity of the (*hkl*) plane and *N* is the number of diffraction peaks. The texture coefficient gives a measure of the orientation of each reflection in comparison to a randomly oriented polycrystalline sample. The value of unity represents random orientation, while a value above unity means preferential orientation in that direction. In this analysis, eight reflections from the cubic PbS structure were considered. Results are presented in Table. As seen from Table, the sample exhibits randomly preferential orientation in the [111], [200], [220] and [400] directions.

Table. Structural parameters of PbS film

hkl	(111)	(200)	(220)	(311)	(222)	(400)	(331)	(420)
TC (hkl)	1.46	1.07	1.09	0.84	0.88	1.11	0.88	0.68
Stand. *d* values	3.426	2.967	2.098	1.789	1.713	1.484	1.361	1.327
d values	3.421	2.966	2.096	1.788	1.711	1.483	1.361	1.326
a (Å)	5.925	5.932	5.928	5.930	5.928	5.932	5.931	5.932

The interplanar spacing *d* were calculated by Bragg's law,

$$n\lambda = 2dsin\theta \tag{3}$$

where n is the order of diffraction, λ is the wavelength of the incident x-ray, θ is the Bragg angle. There are shifts in the d values for PbS sample with respect to the standard values on the basis of PDF Card No: 01-077-0244 data. As shown in Table, observed d values for the sample are smaller than the standard d values. Similar result has been observed in the literature [27].

Lattice constants of PbS film were found using the following formula:

$$a = d_{hkl}\sqrt{h^2 + k^2 + l^2} \tag{4}$$

where a is the lattice constant. The lattice constant values for different orientations of the sample are found to be slightly different as shown in Table. Therefore, it is required to obtain the corrected value of lattice constant. It has been evaluated from two different ways. The first is based on the highest angle reflection data. Different lattice constant values for different orientations are due to the errors in the measurements of the lattice parameter. The systematic error in lattice parameter (a) decreases as θ increases. Therefore, the value of a for the highest angle reflection data is the most accurate than those taken from low angle peaks [28]. This value calculated to be 5.932 Å for the highest angle reflection as shown in Table . The second is based on the Nelson–Riley Function. The true lattice constant value can be determined from the intercept of the Nelson–Riley Function (*NRF*) plot to θ=90° [28]. *NRF* plot is a graph of the calculated values of lattice constant for different orientations versus the NRF function. *NRF* function defined as [26]

$$NRF = \frac{1}{2}\left(\frac{cos^2\theta}{sin\theta} + \frac{cos^2\theta}{\theta}\right) \tag{5}$$

Fig. 2 shows NRF plot of lattice parameter for the PbS film. The corrected value of lattice constant is found to be 5.932 Å which is in agreement with the value of 5.93 A˚ obtained by Mathews et all. [10] and Rajathi et all. [29]. This value is free from systematic errors [30]. The lattice constant values calculated by both methods for the sample are the same. Thus, the first method allows us to determine the value of lattice constant more easily than the Nelson Riley Function method. Deviation of the lattice constant of the PbS film from its bulk value of 5,934 Å confirms that the film is under strain.

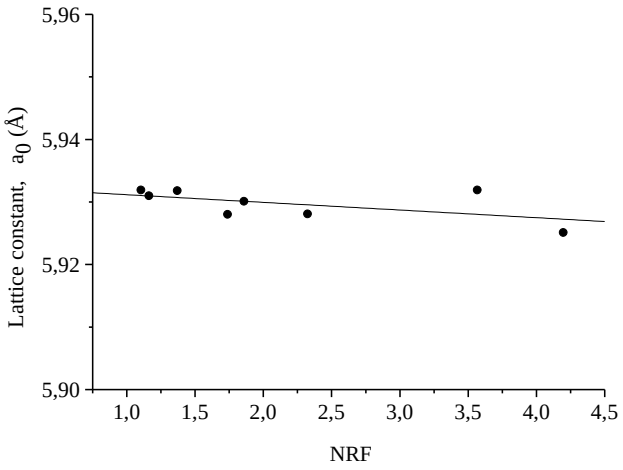


Figure 2. Nelson-Riley plot of lattice parameter for PbS sample

In an unstrained perfect polycrystalline material, all the points for each plane in Nelson–Riley Function (NRF) plot of lattice parameter lie on a straight line. As can be observed in Figure 2, the points do not lie on a straight line. It is said that it is an indication of the strain in the sample. This indication of the strain in the sample could be evaluated as the contraction of the unit cell along the a-axis. The strain which is related to lattice mismatch, deficiencies, defects and concentration of native imperfections depends upon the method used to produce the sample [31, 32]. The strain of the sample has been calculated by the equation:

$$\beta = (\lambda/Dcos\theta) - \varepsilon tan\theta \tag{6}$$

where β is the full width at half maximum of the peak, λ=1.5406Å is the CuK_α radiation wavelength, D is the grain size, and ε is the strain [26]. $\beta \cos\theta/\lambda$ versus $sin\,\theta/\lambda$ plots is indicated in Figure 3 for the PbS film. The slope of the straight line is defined as the mean strain value. The calculated value of the strain is $7.6x10^{-3}$ lines^{-2}m^{-4}. It is an indication of the macrostrain that the diffraction peaks are shifted slightly relative to their normal positions because of the material deformation and that the diffraction peaks are symmetrical as seen from the x-ray diffraction pattern [28]. The macro strain value for PbS sample is in agreement with results of the literature [10, 33].

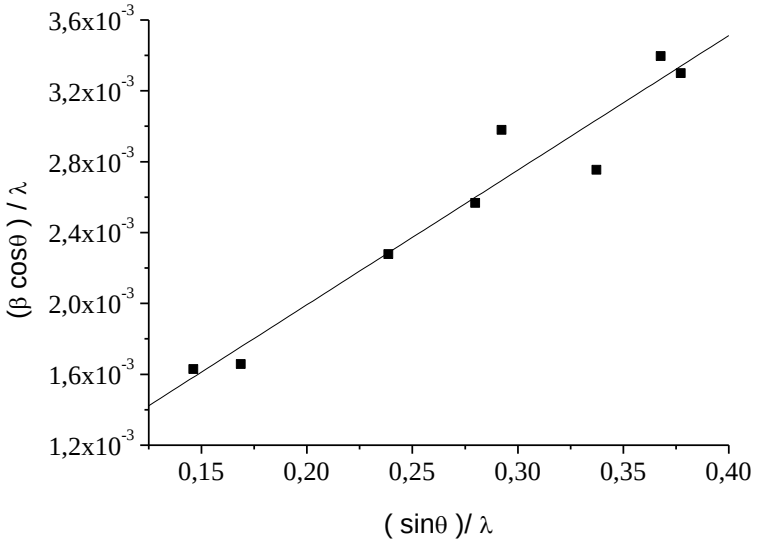


Figure 3. βcosθ/λ versus sinθ/λ plot of PbS sample

The crystallite size has been determined by Scherrer equation [28]:

$$D = 0.9\lambda/(\beta cos\theta) \tag{7}$$

The mean crystallite size of the sample for the planes with randomly preferential orientation was found to be about 45 nm. The crystallite size of the sample indicates that the film is nanostructured. Materials with an average crystallite size not exceeding about 100 nm are generally referred to as nanocrystalline or nanostructured [34]. The mean crystallite size of the sample is comparable with the results of literature [17, 33, 35-37].

The dislocation density (γ) has been calculated by the formula,

$$\gamma = c/D^2 \tag{8}$$

where *c* is usually accepted unity [38]**.** The estimated dislocation density value is found to be $4.9x10^{14}$ lines/m^2. Similar results for PbS film have been observed in the literature [33, 36]**.**

The FESEM image of the PbS film is shown in Figure 4. The FESEM result shows that there is well surface coverage and morphology in various sized irregular triangle and flower-like crystallites. An individual flower-like crystallite has multi facets as shown inside the circle. The grain size measured from FESEM images varies over a broad range from about 40 to 250 nm. These values are bigger than the grain size value of the film estimated from the XRD result indicating that the grains are composed of several crystallites. Small crystallites come together and to form large crystallites with larger grain size which seems to be optimum for photoconductivity of PbS films. Similar results were reported by Tohidi et all. [39], Davar et all. [40] and Pentia et all. [2]. In recent years, flower like PbS films have attracted much attention due to their interesting morphology and potential applications [40]. The PbS film having flowerlike morphology shows a higher electrical conductivity than the other morphologies, which may have potential use in the design of PbS crystals with desirable morphology for the production of thermoelectric devices. [41]. A few papers on flower like PbS films have been reported by Davar et all. [40] and Jin et all. [41].

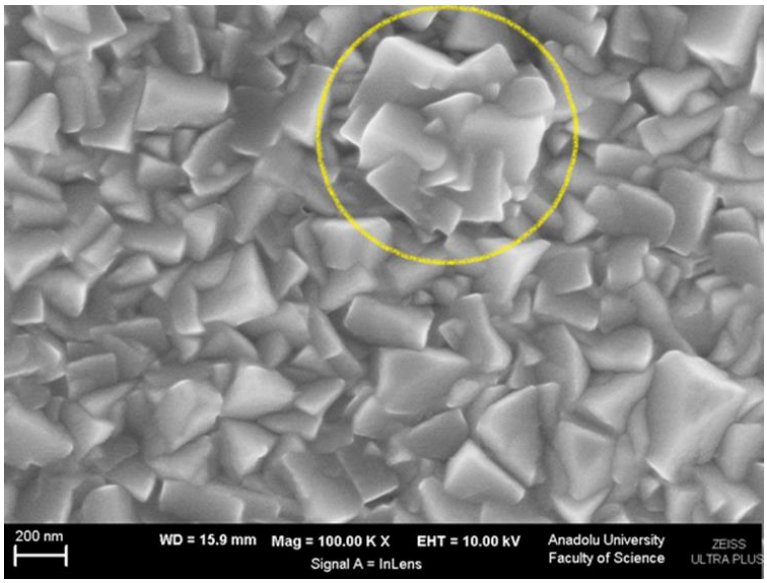


Figure 4. FESEM image of PbS sample

FT-IR spectroscopy technique can be employed to generate a spectroscopic fingerprint for identification and comparison of compounds. In revealing the spectroscopic fingerprints of a new compound, it is quite useful to predict the presence of characteristic functional groups absorbing light in definite frequencies [35]. FT-IR spectra of the PbS sample is shown in Figure 5. The FT-IR spectrum of lead sulfide sample shows eight bands at 474, 663, 778, 948, 1382, 1630, 1936 and 2360 cm^{-1}.The absorption bands at 474, [29, 42] and 948 cm^{-1} [43] are attributed to lead sulfide. The peaks at about 2350-2360 cm^{-1} are due to the asymmetric stretching of carbon dioxide in the air [44]. The absorption peak at 1630 cm^{-1} is assigned to N–H bond [29, 35]. C-H streching peak is observed at 1382 cm^{-1} [35, 45, 46]. The absorption peak around 778 cm^{-1} corresponds to C-O bend [47]. The peak corresponding to the C-S stretch occurs at about 663 cm^{-1} [48]. The presence of various functional groups and PbS bands in the FT-IR study indicate that the material belongs to PbS.

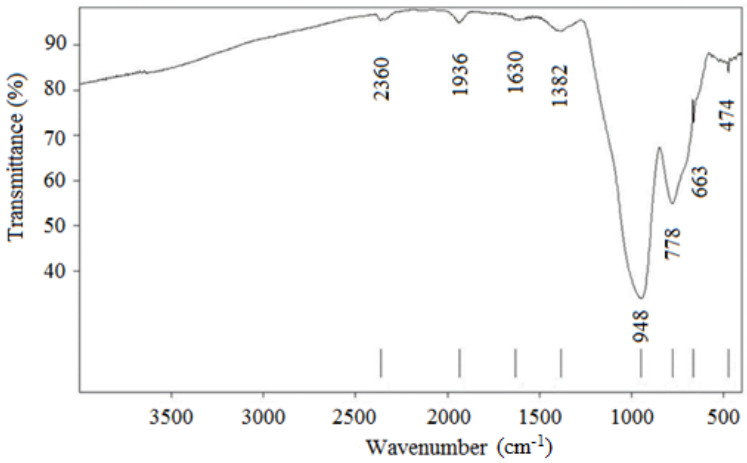


Figure 5. FTIR spectrum of PbS film

Raman spectroscopy is a nondestructive technique commonly used to provide information easily and quickly about molecular vibrations and crystal structures of the materials. Generally, spectrum of a crystalline material shows sharp and intense Raman peaks while amorphous or polycrystalline sample presents broad and less intense Raman peaks [49]. As indicated in Figure 6, the spectrum of PbS shows seven bands at 78, 134, 273, 432, 604, 831 and 966 cm^{-1}. The peak around 78 cm^{-1} is ascribed to the A_{1g} mode in the PbS film [50]. A rather sharp and strong peak around 134 cm^{-1} is probably assigned to the combination of phonon modes which is longitudinal and transverse acoustic [51] or most likely ascribed to the combination of transverse optical and acoustic phonons [52]. This peak is also comparable with the results of Cao et all. [53], Perez et all. [51] and Tohidi et all. [39]. The peak at about 272 cm^{-1} is assigned to two-phonon processes (2x135 = 270 cm^{-1}) of the PbS [53-55]. The peak around 431 cm^{-1} is attributed to the scattering by 2LO phonons localized in PbS [54]. The peaks at 604 and 966 cm^{-1} are assign to the photodegradation of PbS. They are characteristic peaks for the lead oxysulphates according to Batonneau's work [56]. The peak at about 830 cm^{-1} may be originated from the C-C stretch or R-NH2 wag modes [57]. This peak is also comparable with the result of Ramaswamy et all. [58].

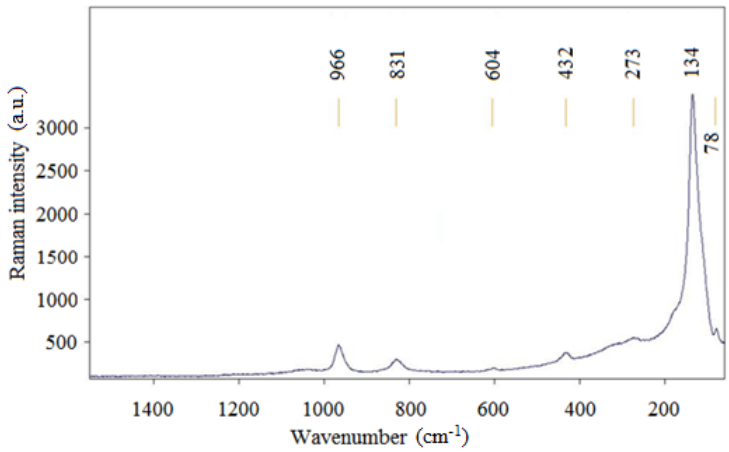


Figure 6. Raman spectrum of PbS film

The optical band gap was calculated by Tauc's equation [59]:

$$\alpha h\nu = A\left(h\nu - E_g\right)^m \tag{9}$$

where A is a constant, E_g is the optical band gap of the material and the exponent m = 1/2 stands for the allowed direct transitions. The $(\alpha h\nu)^2$ versus photon energy $(h\nu)$ plot for the PbS film is linear in fundamental absorption region as it is observed in Figure 7, indicating the direct nature of the optical transition. The straight portion of the curve is extrapolated to the energy axis at $\alpha = 0$, which gives the optical band gap of PbS. The estimated value of the band gap was found to be 1.28 eV.

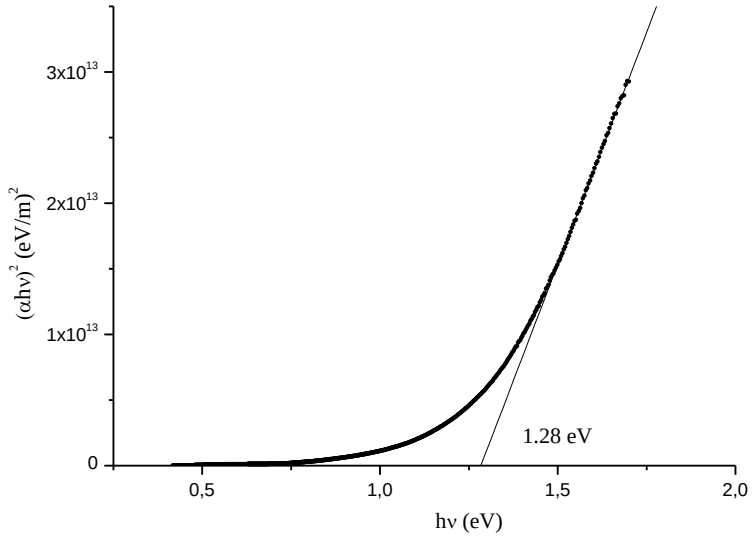


Figure 7. The plot of $(\alpha h\nu)^2$ vs. $(h\nu)$ for PbS film

The value of the band gap for the PbS bulk was 0.41 eV. The optical absorption edge of PbS exhibits a blue shift. This shift of the band gap according to bulk PbS can be attributed to the quantum size effect [45, 60]. Quantization effects are observed when the crystallite size of a semiconductor is near to or less than the bulk Bohr exciton radius. Generally, when the crystallite size of PbS quantum dots decreases to the 5–18 nm range, the band gap of the PbS film increases. According to the effective mass aproximation [61], the optical absorption energy shift of nanostructured material showing quantum confinement effect is given by (neglecting Coulomb interaction):

$$\Delta E_g = E_g(D) - E_{g(bulk)} = \hbar^2\pi^2/2\mu D^2 \tag{10}$$

where $E_g(D)$ is the optical band gap of the nanostructured PbS sample as a function of the crystallite size, $E_{g(bulk)}$ is the band gap of bulk PbS, μ is the reduced effective mass $(m_e^* m_h^*/(m_e^* + m_h^*))$ of the PbS material, m_e^* and m_h^* are the effective masses of the electron and hole, respectively [62]. The reduced effective mass for PbS was taken as $0.0425m_0$, where m_0 is the mass of free electron [63]. The shift of the band gap caused by the crystallite size of 45 nm was found to be 4 meV, which is much smaller than the observed values. Therefore, the crystallite size value of the PbS sample does not allow to explain the shifting of the band gap. Similiar results were reported by Vorobiev [64, 65].

The quantum confinement in this sample is not significant effect because of the crystallite size is greater than 18 nm. Aside from the quantum confinement effect, band gap shift of the PbS film having larger crystallite size may also be caused by different mechanisms such as film thickness, crystallite size, defects, strain, morphology, etc. [15, 37, 62, 65].

4. CONCLUSION

PbS thin films were produced at room temperature of 26°C by simple and cost-effective chemical bath deposition method. XRD analysis revealed that the produced PbS film was polycrystalline having

randomly preferential orientation in the [101], [200], [220] and [400] directions with face centered cubic structure. The lattice constant value is found to be 5.932 Å from NRF plot. The macro strain value of the sample is $7.6x10^{-3}$ lines^{-2}m^{-4}. The mean crystallite size of the nanostructured sample is about 45 nm according to the Scherrer's formula. The estimated dislocation density value of the sample is determined to be $4{,}9x10^{14}$ lines m^{-2}. The FESEM result shows that there is well surface coverage and morphology in various sizes and shapes. XRD study and FESEM image indicate that the produced PbS film has a nano-sized grains. The formation of PbS sample is confirmed by FT-IR and Raman studies. The optical absorption study reveals that the transition of the produced PbS sample is a direct allowed. The band gap of the sample is 1.28 eV which is higher than bulk PbS. The optical band gap shifted to blue makes PbS useful as an absorbing layer for photovoltaic applications.

ACKNOWLEDGMENTS

The author is grateful to Evren Turan from Eskişehir Technical University for their valuable comments and wishes to thank Eskişehir Technical University Faculty of Science for all measurements.

REFERENCES

[1] Androulakis J, Lin C-H, Kong H-J, Uher C, Wu C-I, Hogan T, Cook BA, Caillat T, Paraskevopoulos KM, Kanatzidis MG. Spinodal decomposition and nucleation and growth as a means to bulk nanostructured thermoelectrics: enhanced performance in $Pb_{1-x}Sn_xTe$-PbS. J Am Chem Soc 2007; 129: 9780-9788.

[2] Pentia E, Pintilie L, Matei I, Botila T, Pintilie I. Combined chemical–physical methods for enhancing IR photoconductive properties of PbS thin films. Infrared Phys Techn 2003; 44: 207–211.

[3] Zarubin IV, Markov VF, Maskaeva LN, Zarubina NV and Kuznetsov MV. Chemical sensors based on a hydrochemically deposited lead sulfide film for the determination of lead in aqueous solutions. J Anal Chem+ 2017; 72: 327-332.

[4] Nair P K, Gomezdaza O, Nair MTS, Metal sulphide thin film photography with lead sulphide thin films. Adv Mater Opt Electr 1992; 1: 139–145.

[5] Seo J, Cho MJ, Lee D, Cartwright AN, Prasad PN. Efficient heterojunction photovoltaic cell utilizing nanocomposites of lead sulfide nanocrystals and a low-bandgap polymer. Adv Mater 2011; 23: 3984–3988.

[6] Rogach AL, Gaponik N, Lupton JM, Bertoni C, Gallardo D, Dunn D, Pira N, Paderi M, Reppeto P, Romanov S, O'Dwyer C, Sotomayo C, Eychmuller A. Light emitting diodes with semiconductor nanocrystals. Angew Chem Int Edit 2008; 47: 6538-6549.

[7] Pop I, Nascu C, Ionescu V, Indrea E Bratu I. Structural and optical properties of PbS thin films obtained by chemical deposition. Thin Solid Films 1997; 307: 240-244.

[8] Bakueva L, Musikhin S, Hines MA, Chang TWF, Tzolov M, Scholes GD Sargent EH. Size-tunable infrared (1000-1600) nm electroluminescence from PbS quantum-dot nanocrystals in a semiconducting polymer. Appl Phys Lett 2003; 82: 2895-2897.

[9] Al Din NS, Hussain N, Jandow N. Structural and optical studied of nano structured lead sulfide thin films prepared by the chemical bath deposition technique. Aip Conf Proc 2016; 1758: 020002 (7p).

[10] Mathews NR, Angeles–Chavez C, Cortes-Jacome MA, Toledo-Antonio JA. Physical properties of pulse electrodeposited lead sulfide thin films. Electrochim Acta 2013; 99: 76– 84.

[11] Motlagh Z, Araghi MEA. Effect of film thickness and texture morphology on the physical properties of lead sulfide thin films. Semicond Sci Tech 2016; 31: 025017 (11p).

[12] Chattopadhyay T, von Schnering HG, Grosshans WA, Holzapfel W B. High pressure Xray diffraction study on the structural phase transitions in PbS, PbSe and PbTe with synchrotron radiation. Physica B & C 1986; 139-140: 356-360.

[13] Rafea MA, Roushdy N. Study of optical properties of nanostructured PbS films. Phil Mag Lett 2010; 90: 113-120.

[14] Zheng X, Gao F, Ji F, Wu H, Zhang J, Hu X, Xiang Y. Cu-doped PbS thin films with low resistivity prepared via chemical bath deposition. Mater Lett 2016; 167: 128–130.

[15] Yucel E, Yucel Y. Fabrication and characterization of Sr-doped PbS thin films grown by CBD. Ceram Int 2017; 43: 407–413.

[16] Moreno OP, Perez RG, Portillo MC, Lima LC, Tellez GH, Rosas ER. Morphological, structural, optical and electrical properties of PbS nanocrystals doped with Fe^{2+} grown by chemical bath. Optik 2016; 127: 10273–10282.

[17] Faraj MG. Effect of thickness on the structural and electrical properties of spray pyrolysed lead sulfide thin films. AJCMP 2015; 5: 51-55.

[18] Emeakaroha TM, Ezekoye BA, Ezekoye VA Ighodalo KO. Optical and structural properties of silar-grown highly oriented lead sulphide (PbS) thin films. Chalcogenide Lett 2016; 13: 91-96.

[19] Boadi NO, McNaughter PD, Helliwell M, Malik MA, Awudza JAM, O'Brien P. The deposition of PbS and PbSe thin films from lead dichalcogenoimidophosphinates by AACVD. Inorg Chim Acta 2016; vol. 453: 439–442.

[20] Thirumavalavana S, Mani K, Suresh S. Investigation on structural, optical, morphological and electrical properties of lead sulphide (PbS) thin films. J Ovonic Res 2015; 11: 123-130.

[21] Beddek L, Messaoudi M, Attaf N, Aida MS and Bougdira J. Sulfide precursor concentration and lead source effect on PbS thin films properties. J Alloy Compd 2016; 666: 327-333.

[22] Asenjo B, Guillen C, Chaparro AM, Saucedo E, Bermudez V, Lincot D, Herrero J, Gutierrez MT. Properties of In_2S_3 thin films deposited onto ITO/glass substrates by chemical bath deposition. J Phys Chem Solids 2010; 71: 1629–1633.

[23] Rayaprolu K. Boilers for Power and Process. Boca Raton, USA: CRC Press, 2009.

[24] http://www.subsport.eu/wp-content/uploads/2012/05/alternative-to-hydrtazine-USA-2001-k.pdf, 2018.

[25] Mahmoud S, Hamid O. Growth and characterization of lead-sulfide films deposited on glass substrates. Fizika A 2001; 10: 21–30.

[26] Gurumurugan K, Mangalaraj D, Narayandass SK, Sekar K and Vallabhan CPG. Characterization of transparent conducting CdO films deposited by spray pyrolysis. Semicond Sci Tech 1994; 9: 1827-32.

[27] Sarma MP, Wary G. Effect of molarity on structural and optical properties of chemically deposited nanocrystalline PbS thin film. ILCPA 2017; 74: 22-35.

[28] Cullity BD, Stock SR. Elements of X-ray Diffraction. New Jersey, USA: Pearson Prentice Hall, 2001.

[29] Rajathi S, Kirubavathi K, Selvaraju K. Structural, morphological, optical, and photoluminescence properties of nanocrystalline PbS thin films grown by chemical bath deposition. Arab J Chem 2017; 10: 1167–1174.

[30] Whiston C, Prichard E. X-ray Methods. New York, USA: John Wiley and Sons Ltd, 1987.

[31] Begum A, Hussain A, Rahman A, Effect of deposition temperature on the structural and optical properties of chemically prepared nanocrystalline lead selenide thin films. Beilstein J Nanotech 2012; 3: 438–443.

[32] Desai SP, Suryawanshi MP, Bhosale SM, Kim JH, Moholkar AV. Influence of growth temperature on the physico-chemical properties of sprayed cadmium oxide thin films. Ceram Int 2015; 41: 4867-4873.

[33] Rajashree C, Balu AR. Tuning the physical properties of PbS thin films towards optoelectronic applications through Ni doping. Optik 2016; 127: 8892–8898.

[34] Sadovnikov SI, Gusev AI, Rempel AA. Nanostructured lead sulfide: synthesis, structure and properties. Russ Chem Rev 2016; 85: 731-758.

[35] Kumar D, Agarwal G, Tripathi B, Vyas D, Kulshrestha V. Characterization of PbS nanoparticles synthesized by chemical bath deposition. J Alloy Compd 2009; 484: 463-466.

[36] Touati B, Gassoumi A, Dobryden I, Natile MM, Vomiero A, Turki NK. Engineering of electronic and optical properties of PbS thin films via Cu doping. Superlattices Microstruct 2016; 97: 519-528.

[37] Hone FG, Dejene FB. Synthesis and characterization of lead sulphide thin films from ethanolamine (ETA) complexing agent chemical bath. Mater Res Express 2018; 5: 026409 (9p).

[38] Williamson GB, Smallman RC. Dislocation densities in some annealed and cold-worked metals from measurements on the x-ray Debye-Scherrer spectrum. Philos Mag A: Series 8 1956; 1: 34-46.

[39] Tohidi T, Jamshidi-Ghaleh K, Namdar A, Abdi-Ghaleh R. Comparative studies on the structural, morphological, optical, and electrical properties of nanocrystalline PbS thin films grown by chemical bath deposition using two different bath compositions. Mat Sci Semicon Proc 2014; 25: 197-206.

[40] Davar F, Mohammadikish M, Loghman-Estarki MR, Masteri-Farahani M. Synthesis of micro-and nanosized PbS with different morphologies by the hydrothermal process. Ceram Int 2014; 40: 8143-8148.

[41] Jin R, Chen G, Wang Q, Pei J, Wang G, Wang L. Flowerlike PbS microcrystals: citric acid assisted synthesis, shape evolution, and electrical conductivities. Eur J Inorg Chem 2010; 2010: 5700–5708.

[42] Kalita PK, Das B, Devi R. Effect of growth temperature on chemical synthesis of PbS quantum dots", Int Res J Pure Appl Chem 2014; 4: 97-107.

[43] Chernyshova IV. Anodic processes on a galena (PbS) electrode in the presence of n-butyl xanthate studied FTIR-spectroelectrochemically. JPC B 2001; 105: 8185-8191.

[44] Giansante C, Carbone L, Giannini C, Altamura D, Ameer Z, Maruccio G, Loiudice A, Belviso MR, Cozzoli PD, Rizzo A, Gigli G. Colloidal arenethiolate-capped PbS quantum dots: optoelectronic properties, self-assembly and application in solution-cast photovoltaics. JPC C 2013; 117: 13305-13317.

[45] Ye J, Sun L, Gao S. Fabrication of hollow PbS nanospheres and application in phenol release. Springerplus 2013; 2: 323 (6p).

[46] Navaneethan M, Nisha KD, Ponnusamy S, Muthamizhchelvan C. Optical and surface morphological properties of triethylamine passivated lead sulphide nanoparticles. Mater Chem Phys 2009; 117: 443–447.

[47] Gulley-Stahl HJ, Haas JA, Schmidt KA, Evan AP, Andre JS., Attenuated total internal reflectance infrared spectroscopy (ATR-FTIR): a quantitative approach for kidney stone analysis. Appl Spectrosc 2009; 63: 759–766.

[48] Szendrei K, Gomulya W, Yarema M, Heiss W, Loi M. PbS nanocrystal solar cells with high efficiency and fill factor. Appl Phys Lett 2010; 97: 203501 (3p).

[49] Chen J-H, Chao C-G, Ou J-C, Liu T-F. Growth and characteristics of lead sulfide nanocrystals produced by the porous alumina membrane. Surface Science 2007; 601: 5142-5147.

[50] Hangyo M, Nakashima S, Hamada Y, Nishio T. Raman scattering from the misfit-layer compounds $SnNbS_3$, $PbNbS_3$, and $PbTiS_3$. Phys Rev B 1993; 48: 11291-11297.

[51] Perez RG, Tellez GH, Rosas UP, Torres AM, Tecorralco JH, Lima LC, Moreno OP. Growth of PbS nanocrystals thin films by chemical bath. JMSE-A 2013; 3: 1-13.

[52] Sherwin R, Clark RJH, Lauck R, Cardona M. Effect of isotope substitution and doping on the Raman spectrum of galena (PbS). Solid State Commun 2005; 134: 565-570.

[53] Cao H, Wang G, Zhang S, Zhang X. Growth and photoluminescence properties of PbS nanocubes. Nanotechnology 2006; 17: 3280-3287.

[54] Milekhin A, Sveshnikova L, Duda T, Surovtsev N, Adichtchev S, Zahn DRT., "Optical phonons in nanoclusters formed by the Langmuir-Blodgett technique. Chinese J Phys 2011; 49: 63-70.

[55] Krauss TD, Wise FW, Tanner DB. Observation of coupled vibrational modes of a semiconductor nanocrystal. Phys Rev Lett 1996; 76: 1376-1379.

[56] Batonneau Y, Bremard C, Laureyns J, Merlin JC. Microscopic and imaging Raman scattering study of PbS and its photo-oxidation products. J Raman Spectrosc 2000; 31: 1113-1119.

[57] Lynch M. An investigation of solutions of sulfur in oleylamine by Raman spectroscopy and their relation to lead sulfide quantum dot synthesis. Undergraduate honors theses, University of Colorado, Boulder, Colorado, USA, 2017.

[58] Ramaswamy S, Rajaram RK, Ramakrishnan V. Infrared and laser Raman spectra of bis(DL-methioninium) sulfate. J Raman Spectrosc 2005; 36: 840-847.

[59] Pankove JI. Optical Process in Semiconductors. New York, USA: Dover, 1975.

[60] Pawar SB, Shaikh JS, Devan RS, Ma YR, Haranath D, Bhosale PN, Patil P S. Facile and low cost chemosynthesis of nanostructured PbS with tunable optical properties. Appl Surf Sci 2011; 258: 1869-1875.

[61] Brus LE. Electron-electron and electron-hole interactions in small semiconductor crystallites: The size dependence of the lowest excited electronic state. J Chem Phys 1984; 80: 4403-4409.

[62] Thareja RK, Mohanta A. ZnO Nanoparticles, In: Sattler KD, editor. Handbook of Nanophysics: Nanoparticles and Quantum Dots. Boca Raton, USA: CRC Press, 2011.

[63] Singh J. Physics of Semiconductors and Their Heterostructures. Singapore: McGraw-Hill, 1993.

[64] Vorobiev YV, Horley PP, Hernandez-Borja J, Esparza-Ponce HE, Ramirez-Bon R, Vorobiev P, Perez C, Gonzalez-Hernandez J. The effects of porosity on optical properties of semiconductor chalcogenide films obtained by the chemical bath deposition. Nanoscale Res Lett 2012; 7: 483 (5 p).

[65] Yeon DH, Lee SM, Jo YH, Moon J, Cho YS. Origin of the enhanced photovoltaic characteristics of PbS thin film solar cells processed at near room temperature. J Mater Chem A 2014; 2: 20112-20117.